Regular Article – Theoretical Physics

Systematics of half-lives for proton radioactivity

E.L. Medeiros[a], M.M.N. Rodrigues, S.B. Duarte, and O.A.P. Tavares

Centro Brasileiro de Pesquisas Físicas - CBPF/MCT, Rua Dr. Xavier Sigaud 150, 22290-180 Rio de Janeiro-RJ, Brazil

Abstract. Half-life measurements for both ground-state and isomeric transitions in proton radioactivity are systematized by using a semiempirical, one-parameter model based on tunneling through a potential barrier, where the centrifugal and overlapping effects are taken into account within the spherical nucleus approximation. This approach, which has been successfully applied to alpha decay cases covering ~ 30 orders of magnitude in half-life, has shown, in addition, very adequate at fitting all existing data on partial half-life, $T_{1/2_\mathrm{p}}$, of proton emission from nuclei. Nearly 70 measured half-life values have been analysed, and the data could be described by two straight lines relating the pure Coulomb contribution to half-life with the quantity $Z_\mathrm{d}(\mu_0/Q_\mathrm{p})^{1/2}$ (Z_d is the atomic number of the daughter nucleus, μ_0 is the reduced mass, and Q_p is the total nuclear energy available for decay). These straight lines are shown to correspond to different degrees of deformation, namely, very prolate ($\delta \gtrsim 0.1$), and other shaped ($\delta \lesssim 0.1$) parent nuclei. The goodness in reproducing the data attained in the present systematics allows for half-life predictions for a few possible cases of proton radioactivity not yet experimentally accessed.

PACS. 23.50.+z Decay by proton emission

1 Introduction

Proton decay, the radioactive process by which nuclei disintegrate by the emission of a proton, has been detected and analysed since its first observation from the proton-unstable isomer $^{53\mathrm{m}}$Co in September 1970 by Jackson *et al.* [1], and promptly confirmed by Cerny *et al.* [2]. It is a case of artificial radioactivity for the proton-emitter nuclides are located very far from the beta-stability line, in the region of very neutron-deficient nuclides, near the so-called proton drip line. The Q-value for the ground-state and isomeric proton transitions, Q_p, does not exceed a few units of MeV ($Q_\mathrm{p} \lesssim 2\,\mathrm{MeV}$), and the half-lives for the cases measured so far are found in the range $\sim 3\,\mu\mathrm{s}$–$17\,\mathrm{s}$ [3–5].

For proton emission to occur the valence proton must tunnel a potential barrier comprising the superposition of the Coulomb and centrifugal barriers (see fig. 1). The former potential is relatively low and the latter one is relatively high when comparing with the alpha decay case, thus making proton decay rates strongly sensitive to the values of the angular momentum ℓ associated to the proton transition. In the proton decay of nuclei the overlapping region is, in general, very narrow as compared with the separation region (fig. 1), implying that the penetrability through the barrier comes essentially from the external (Coulomb-plus-centrifugal) barrier. Since Gamow's
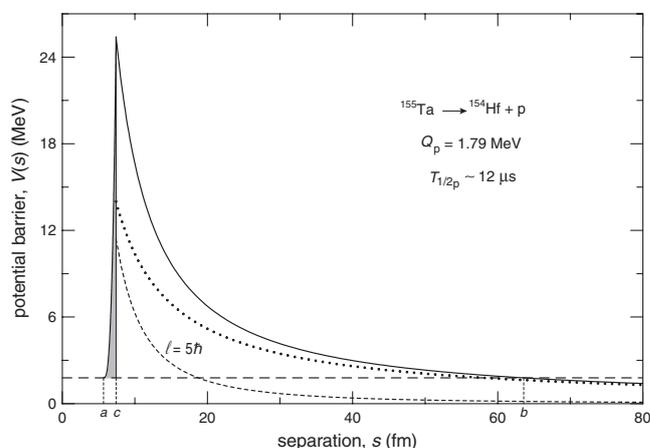
[a] e-mail: emil@cbpf.br

Fig. 1. The one-dimensional potential barrier, $V(s)$, for a typical proton decay case. In the external region c–b the total potential barrier (full line) comprises superposition of the Coulomb (dotted line) and centrifugal (short-dashed line) barriers. The overlapping region a–c is emphasized by the shaded area. The horizontal dashed line indicates the Q_p-value.

factor calculated in the overlapping region, G_ov, is small it results that the "arrival" of the proton to be emitted at the nuclear surface is close to unity ($0.75 \lesssim \mathrm{e}^{-G_\mathrm{ov}} \lesssim 1$), thus differing appreciably from the emission of a cluster of nucleons such as an alpha particle one, for which case

Table 1. Number of measurements, cases, and types of deformed parent nuclei considered in the present systematic analysis.

Values of ℓ	Total number of Measurements	Number of cases					
		Nuclear shape			Energy state		
		Large prolate	Other	Total	Ground	Isomeric	Total
0	11	1	7	8	6	2	8
2	24	7	7	14	11	3	14
3	5	3	0	3	3	0	3
4	1	1	0	1	0	1	1
5	29	1	16	17	7	10	17
9	1	0	1	1	0	1	1
Totals	71	13	31	44	27	17	44

$e^{-G_{\rm ov}}$ can be as low as units of 10^{-3} or even less [6]. In addition, in recent past considerable theoretical efforts have provided a much better understanding on the proton preformation probability at the nuclear surface in terms of deformation and pairing effects as reported, for instance, in refs. [7–11] and in a number of papers quoted therein.

Ground- and isomeric-state proton radioactive nuclei have been produced from heavy-ion fusion-evaporation reactions with moderate-energy (~ 4–$6\,{\rm MeV/u}$), neutron-deficient projectiles and target nuclei [12–16]. In such reactions a number of exotic proton-emitter nuclides have been populated coming from $1{\rm p}xn$ successive evaporation channels in the excited compound nuclei. Hofmann et al. [17] from the GSI (Darmstadt) were the first who observed in ^{151}Lu a proton decay from the ground state and measured a half-life of $(85 \pm 10)\,{\rm ms}$. This experiment was followed by the detection of a proton line of half-life $(0.42 \pm 0.10)\,{\rm s}$ ascribed to a direct proton decay of the ^{147}Tm isotope [18]. Since then a number of proton decay half-life measurements have been reported, and the data have been summed to a total of 71 measured half-life values for 27 different cases of ground-state proton radioactivity plus other 17 cases of isomeric proton transitions up to now [3–5,7,11,19–23] (see table 1). No cases of $Z \leqslant 50$ parent nuclei for ground-state proton emission have been observed to date at all. Progresses in proton radioactivity investigation covering both experimental and theoretical aspects can be found in refs. [5,12–16] and [4,9–11,22,23], respectively. The frontiers of the knowledge related to this unusual phenomenon, such as deformed proton emitters, fine structure, excited states, competition between proton emission and rotation, non-adiabatic models, and others, can be appreciated additionally in refs. [24–31].

Recently, we have developed a one-parameter model for the alpha decay process, whose model is based on the quantum-mechanical tunneling mechanism of penetration through a potential barrier, where both the centrifugal and overlapping effects have been taken into account [6]. This approach enabled us to calculate and systematize the alpha decay half-lives of ground-state to ground-state transitions of mutual angular momentum $\ell = 5$ for all the possible alpha-emitting bismuth isotopes which can be produced by nuclear reactions. In particular, the alpha

decay half-life for the naturally occurring ^{209}Bi isotope was evaluated as $(1.0 \pm 0.3) \times 10^{19}$ years [6], in substantial agreement with the experimental result $((1.9 \pm 0.2) \times 10^{19}$ years [32]). This semiempirical model was, in addition, used to evaluate the half-life of the Pt isotopes [33] where, for the important case of the naturally occurring ^{190}Pt isotope (the radiogenic parent in the ^{190}Pt $\rightarrow$ ^{186}Os dating system), the model yielded a half-life-value of $(3.7 \pm 0.3) \times 10^{11}$ years which is comparable to the alpha decay half-life value of $(3.2 \pm 0.1) \times 10^{11}$ years obtained in the last direct counting experiment to measure the alpha activity of ^{190}Pt isotope [34].

The proposed model mentioned above has also shown to be successfully applicable to a number of isotopic sequences of alpha-emitter nuclides [6,33], and, therefore, it has been used to systematize the alpha-decay half-lives of all known cases of ground-state–to–ground-state alpha transitions of mutual angular momentum $\ell = 0$ [35]. Besides, the predictive power of the model was demonstrated quite recently in discussing the rarest case of natural alpha activity ever observed due to the ^{180}W isotope, for which case the evaluated half-life value of 1.0×10^{18} years [36] matches quite completely with the measured values of $1.1^{+0.8}_{-0.4} \times 10^{18}$ years [37] and $1.0^{+0.7}_{-0.3} \times 10^{18}$ years [38]. The model has served, in addition, to explain quantitatively the very recent observation of an extremely rare alpha activity due to the ^{151}Eu isotope ($T_{1/2_\alpha} = 5^{+11}_{-3} \times 10^{18}$ year [39]) for which case one obtained by the referred model the value 8.5×10^{18} year for the alpha decay half-life of ^{151}Eu [40].

Quite recently, Delion et al. [4] have reported a very simple formula to systematize the partial half-life data of proton emission from nuclei. In their analysis the half-life is corrected by the centrifugal barrier term, and such reduced data are plotted against the Coulomb parameter showing that the data could be fitted to two straight lines corresponding to two groups of parent nuclei of different degrees of nuclear deformation independently of the ℓ-values. The data analysis by Delion et al. [4] allows one to understand in a quantitative way the influence of nuclear deformation on proton radioactivity.

The facts mentioned above have stimulated us to extend our quantum-mechanical tunneling treatment of

alpha decay in systematizing all cases of ground-state and isomeric proton decay half-lives, $T_{1/2_p}$, so far experimentally investigated. Data reduction and analysis procedures have followed to some extent the methodology proposed by Delion *et al.* [4]. Finally, based on this present systematic study, evaluations of half-life for possible new proton emitters not yet observed can be of great importance for new experiments on this line. Thus, we thought it worthwhile to perform a systematic study of proton decay for parent proton-rich nuclei of $Q_p > 0$ for both measured and possible of being measured cases.

2 Semiempirical treatment to proton radioactivity

The one-parameter model reported in details for the alpha decay process [6,33,35] is simple in nature, and the assumption is made of spherical nuclei approximation. In this connection, it is worthwhile to mention that the state of art of the spherical approximation to proton radioactivity can be appreciated in the paper by Åberg *et al.* [8], who investigated various theoretical approaches for describing the ground-state proton emission, where a quantitative agreement with experimental data for spherical proton emitters has been found. Here, the necessary changes are introduced into our original calculation model [6] to adapt it to the proton decay cases. In brief, the decay constant, λ, is calculated as

$$\lambda = \lambda_0 S_p P_{se}, \qquad S_p = e^{-G_{ov}}, \qquad P_{se} = e^{-G_{se}}, \quad (1)$$

where λ_0 is the frequency factor which represents the number of assaults on the barrier per unit of time, S_p is the probability of finding a proton at the nuclear surface, G_{ov} is Gamow's factor calculated in the overlapping barrier region where the proton drives away from the parent nucleus until the configuration at contact is reached, P_{se} is the penetrability factor through the external barrier region as shown in fig. 1, and G_{se} is Gamow's factor calculated in this external, separation region. This latter extends from the contact configuration at $c = R_d + r_p$ up to the separation point where the total potential energy equals the Q_p-value for decay, *i.e.*, the outer turning point (b, in fig. 1). R_d stands for the radius of the daughter nucleus, and r_p is the proton radius. The quantity λ_0 is usually evaluated as $\lambda_0 = \frac{v}{2a}$, where v is the relative velocity of the emitting proton and the daughter nucleus, and $a = R_p - r_p$ is the inner turning point, *i.e.*, the difference between the radius of the parent nucleus and the proton radius. The quantity $c - a$ represents, therefore, the extension of the overlapping region.

In cases for which the proton transition goes from the ground or isomeric state of the parent nucleus to the ground state of the daughter nucleus, and expressing lengths in fm, masses in u and energies in MeV, and using the values for the different physical constants, as well as the appropriate conversion factors to maintain coherence in the units, the expressions for G_{ov} and G_{se} transform to

$$G_{ov} = 0.4374702(c-a)g\sqrt{\mu_0 Q_p}\,H(x,y), \qquad (2)$$

where

$$H(x,y) = (x + 2y - 1)^{1/2}, \qquad (3)$$

and

$$G_{se} = 0.62994186\, Z_d \left(\frac{\mu_0}{Q_p}\right)^{1/2} F(x,y), \qquad (4)$$

where

$$F(x,y) = \frac{x^{1/2}}{2y} \times \ln \frac{x^{1/2}H(x,y) + x + y}{\sqrt{x+y^2}}$$

$$+ \arccos \left[\frac{1}{2}\left(1 - \frac{y-1}{\sqrt{x+y^2}}\right)\right]^{1/2} - \frac{H(x,y)}{2y}. \qquad (5)$$

In the above expressions the quantities x and y are defined as

$$x = \frac{20.9008\,\ell(\ell+1)}{\mu_0 c^2 Q_p}, \qquad y = \frac{1}{2}\frac{Z_d e^2}{c Q_p},$$

$$e^2 = 1.4399652\,\text{MeV}\cdot\text{fm}, \qquad (6)$$

where μ_0 represents the reduced mass of the disintegration system, and l is the mutual orbital angular momentum resulting from the centrifugal barrier associated with the rotation of the proton and daughter nucleus around their common centre of mass. As has been explained in [6] eq. (2) results from a combination of power functions in describing both the effective reduced mass, $\mu(s)$, and the potential energy, $V(s)$, in the overlapping region ($a \leqslant s \leqslant c$), *i.e.*,

$$\mu(s) = \mu_0 \left(\frac{s-a}{c-a}\right)^p, \qquad p \geq 0, \qquad (7)$$

$$V(s) - Q_p = Q_p(x+2y-1)\left(\frac{s-a}{c-a}\right)^q, \qquad q \geq 1, \quad (8)$$

where s is the separation between the centres of the proton and daughter nucleus. In calculating Gamow's factor by the classical WKB-integral approximation in the overlapping region,

$$G = \frac{2}{\hbar}\int_a^c \sqrt{2\mu(s)\big[V(s) - Q_p\big]}\,\mathrm{d}s, \qquad (9)$$

eq. (2) emerges, where

$$g = \frac{2}{p+q+2}, \qquad 0 < g \leqslant 2/3 \qquad (10)$$

is the adjustable parameter of the model. Expression (4) is, on the other hand, the usual Gamow's factor in the external region $c - b$ comprising both the Coulomb and centrifugal potential barriers. Note that the parameter g (although very small in proton decay) is related to the unknown strenght of the potential in the overlapping region, the value of which being thus determined from the experimental data of partial proton decay half-lives considered in the systematics.

The values for the quantities μ_0 and Q_p have been calculated from the most recent atomic mass-excess (ΔM)

evaluation [41], and they include the effect of the screening to the nucleus caused by the surrounding electrons. Accordingly, the expressions for μ_0 and Q_p read

$$\frac{1}{\mu_0} = \frac{1}{m_d} + \frac{1}{m_p}, \tag{11}$$

$$m_d = A_d + \frac{\Delta M_d}{F} - \left(Z_d m_e - \frac{10^{-6} k Z_d^\beta}{C}\right), \tag{12}$$

$$Q_p = \Delta M_p - (\Delta M_d + \Delta M) + 10^{-6} k \left(Z_p^\beta - Z_d^\beta\right), \tag{13}$$

where $m_p = 1.00727646676\,\mathrm{u}$ is the proton mass, $m_e = 0.548579911 \times 10^{-3}\,\mathrm{u}$ is the electron rest mass, $C = 931.494009\,\mathrm{MeV/u}$ is the mass-energy conversion factor and $\Delta M = 7.288983386\,\mathrm{MeV}$ is the proton mass excess. The quantity $k Z^\beta$ represents the total binding energy of the Z electrons in the atom, where the values $k = 8.7\,\mathrm{eV}$ and $\beta = 2.517$ for nuclei of $Z \geq 60$, and $k = 13.6\,\mathrm{eV}$ and $\beta = 2.408$ for $Z < 60$ have been derived from data reported by Huang et al. [42].

The value for the proton radius adopted in the present systematics is $r_p = 0.87 \pm 0.02\,\mathrm{fm}$ as it comes from the average of proton radius values in various experiments and analyses of data on elastic electron scattering from hydrogen target [43–47].

The spherical nucleus approximation has been adopted to the present calculation model, and the nuclear radii for the parent, R_p, and daughter, R_d, nuclei have been evaluated following the droplet model of atomic nuclei [48,49], from which the following radius expressions have been used throughout:

$$R_i = \frac{Z_i}{A_i} R_{pi} + \left(1 - \frac{Z_i}{A_i}\right) R_{ni}, \quad i = \mathrm{p, d}, \tag{14}$$

where the radii R_{ji} are given by

$$R_{ji} = r_{ji} \left[1 + \frac{5}{2}\left(\frac{w}{r_{ji}}\right)^2\right], \quad j = p, n; \quad i = \mathrm{p, d}, \tag{15}$$

in which $w = 1\,\mathrm{fm}$ is the diffuseness of the nuclear surface, and the radii r_{ji} represent the equivalent sharp radius of the proton ($j = p$) or neutron ($j = n$) density distribution. These latter quantities, in turn, are calculated following the finite-range droplet model description of nuclei by Möller et al. [49], thus giving

$$r_{pi} = r_0 \left(1 + \overline{\epsilon_i}\right) \left[1 - \frac{2}{3}\left(1 - \frac{Z_i}{A_i}\right)\left(1 - \frac{2Z_i}{A_i} - \overline{\delta_i}\right)\right] A_i^{1/3}, \tag{16}$$

$$r_{ni} = r_0 \left(1 + \overline{\epsilon_i}\right) \left[1 + \frac{2}{3}\frac{Z_i}{A_i}\left(1 - \frac{2Z_i}{A_i} - \overline{\delta_i}\right)\right] A_i^{1/3}, \tag{17}$$

where

$$\overline{\epsilon_i} = \frac{1}{4\,\mathrm{e}^{0.831 A_i^{1/3}}} - \frac{0.191}{A_i^{1/3}} + \frac{0.0031 Z_i^2}{A_i^{4/3}}, \tag{18}$$

$$\overline{\delta_i} = \left(1 - \frac{2Z_i}{A_i} + 0.004781\frac{Z_i}{A_i^{2/3}}\right) \bigg/ \left(1 + \frac{2.52114}{A_i^{1/3}}\right), \tag{19}$$
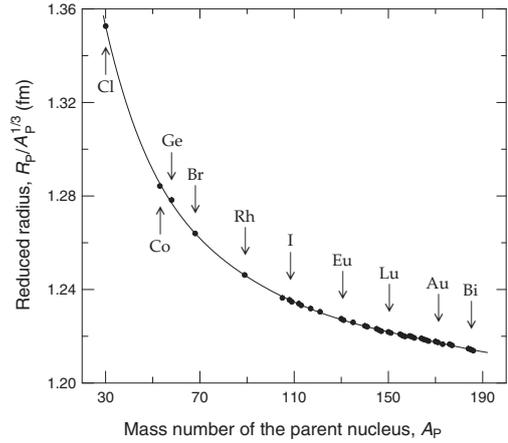

Fig. 2. Reduced radius, $R/A^{1/3}$, plotted against mass number, A, for the parent nuclei considered in the present analysis. Radius values have been calculated following the droplet model of atomic nuclei by Möller et al. [49]. See text for details.

$r_0 = 1.16\,\mathrm{fm}$, and, as before, $i = \mathrm{p}$ (parent) or d (daughter). The radius values for the parent and daughter nuclei evaluated as explained above have been shown to work quite satisfactorily when applied to the alpha decay systematics [6,33,35]. This radius parametrization is valid for nuclei of mass number $A \gtrsim 20$ [49]. Figure 2 shows the variation of the reduced radius $R/A^{1/3}$ of the equivalent liquid-drop model for the parent, proton-emitter nuclides considered in the present work (identical result holds for the daughter nuclei, although not shown in fig. 2). The trend reveals a decreasing by 5–6% in $R/A^{1/3}$ when one passes from Co to Bi along the nuclide region in the vicinity of the proton drip line, thus reflecting some degree of nuclear compressibility.

The observation of the proton-unstable isomer $^{53\mathrm{m}}\mathrm{Co}$ early in 1970 [1,2] opened a new nuclear research field, the artificial proton radioactivity. Subsequently, beside the experimental investigation on ground-state proton decay, a number of cases for isomeric proton transitions have also been detected. We have applied the same approach and methodology described here to analyse and evaluate the half-life values for all known isomeric proton transitions. These have been systematized together with the cases for ground-state proton transitions, thus constituting in a unique set of input data, as will be detailed in the next sections.

3 Data reduction and analysis

The input data to the present systematics comprise all available information on experimental half-life, $T_{1/2_p}^e$, and angular momentum, ℓ, assigned to the respective proton transition. As mentioned in sect. 1, these amount to seventy-one half-life measurements distributed into fourty-four different cases (twenty-seven of ground-state transitions plus seventeen of isomeric-state transitions) of proton emitters from $^{53\mathrm{m}}\mathrm{Co} \to {}^{52}\mathrm{Fe}$ ($T_{1/2_p}^e = 16.5\,\mathrm{s}$,

$\ell = 9$) up to ^{185m}Bi ($T^e_{1/2_p} \approx 52\,\mu\text{s}$, $\ell = 0$), most of them taken from refs. [3–5,11–23,50–61] and references quoted therein. Altogether, the data were classified into four groups: eight cases of $\ell = 0$ (eleven measurements), fourteen cases of $\ell = 2$ (twenty-four measurements), three cases of $\ell = 3$ (five measurements), and seventeen cases of $\ell = 5$ (twenty-nine measurements) plus two isolated cases, namely, ^{117m}La ($\ell = 4$) and the already mentioned ^{53m}Co ($\ell = 9$) proton emitters. The data have been in addition classified according to the degree of deformation (large prolate or other shaped) of the parent nuclei (see table 1) in order to study the effect of deformation in analysing these data with an approach which considers *a priori* nuclei as being spherical.

The partial, proton decay half-life data have been analysed here in a way resembling the systematic study of proton emission by Delion *et al.* [4], but the present one is entirely based on the formalism of the precedent section. Thus, starting from eq. (1), the half-life can be expressed as

$$\tau = \log_{10} T_{1/2_p} = \tau_0 + \tau_1 + \tau_2, \tag{20}$$

where

$$\tau_0 = -22 + \log_{10}\left[a\left(\mu_0/Q_p\right)^{1/2}\right] \tag{21}$$

is the term related to the frequency of assaults on the barrier,

$$\tau_1 = 0.19(c-a)g\sqrt{\mu_0 Q_p}\,H(x,y) \tag{22}$$

is the contribution from the overlapping barrier region, and

$$\tau_2 = 0.27358027 Z_d\left(\frac{\mu_0}{Q_p}\right)^{1/2}\cdot F(x,y) \tag{23}$$

is the one corresponding to the external, separation barrier region. The "penetrability" function, $F(x,y)$, as given by eq. (5), is now expanded in power series of x such that

$$F(x,y) = F(0,y) + F'(0,y)\,x + \text{higher-order terms} \tag{24}$$

with

$$F(0,y) = \arccos(2y)^{-1/2} - (2y-1)^{1/2}/(2y) \tag{25}$$

and

$$F'(0,y)\,x = \frac{(2y-1)^{1/2}}{4y^2}\,x. \tag{26}$$

This makes possible to separate the Coulomb (τ_2^{co}) and centrifugal (τ_2^{ce}) contributions from each other in the external barrier region such that

$$\tau_2 = \tau_2^{co} + \tau_2^{ce}, \tag{27}$$

where

$$\tau_2^{co} = 0.27358027\,Z_d\left(\frac{\mu_0}{Q_p}\right)^{1/2}\times F(0,y)\quad\text{and} \tag{28}$$

$$\tau_2^{ce} = 2.75767886\,\ell(\ell+1)\,Z_d^{-1}\left[(2y-1)Q_p/\mu_0\right]^{1/2}. \tag{29}$$

For all cases of proton emission considered in the present analysis the condition $0 \leqslant x/y^2 < 1$ is satisfied (except
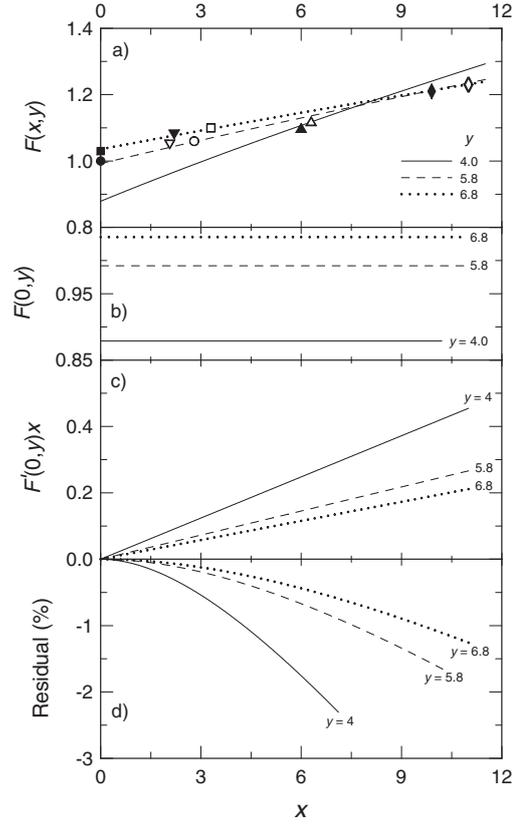

Fig. 3. "Penetrability" function, $F(x,y)$, defined by eqs. (5), (6), and (3) plotted *vs. x* for three values of y as indicated. In a) the points locate a few examples for proton decay cases as follows: $\triangle$, ^{165m}Ir; $\blacktriangle$, ^{164m}Ir; $\bigcirc$, ^{113}Cs; $\blacklozenge$, ^{156m}Ta; $\bullet$, ^{176}Tl; $\triangledown$, ^{147m}Tm; $\square$, ^{112}Cs; $\blacksquare$, ^{167}Ir; $\blacktriangledown$, ^{156}Ta; $\diamondsuit$, ^{147}Tm. b) shows the first term (the purely Coulomb contribution) of the series expansion of $F(x,y)$. c) shows the first-order contribution to $F(x,y)$ which is due to the centrifugal barrier (a term proportional to $\ell(\ell+1)$), and d) is the fraction of $F(x,y)$ (in percent) which is disregarded in composing $F(x,y)$. This latter shows indeed to be very small. Note that the y-values chosen to construct these plots cover the majority of the proton decay cases analysed in this work.

for ^{53m}Co proton emitter), and the residuals in the series expansion (24) of $F(x,y)$ due to higher-order terms can be safely neglected as explained in fig. 3.

Defining a "reduced" half-life as

$$\tau_r = \tau - \left(\tau_0 + \tau_1 + \tau_2^{ce}\right), \tag{30}$$

means that τ_r should contain only the pure Coulomb contribution to half-life, and, therefore, one should expect τ_r not to be dependent upon angular momentum, ℓ, in a plot of τ_r against parameter $\chi = Z_d(\mu_0/Q_p)^{1/2}$. This treatment looks like Delion's *et al.* [4] analysis, and the experimental τ_r^e-values are displayed in fig. 4 (points) for the proton emission cases listed in tables 2 and 3. The data in fig. 4 resulted clearly arranged along two straight lines, the upper one being related to the largely prolate deformed proton emitter nuclides, and a lower one associated to other shaped parent nuclei. As said before, both
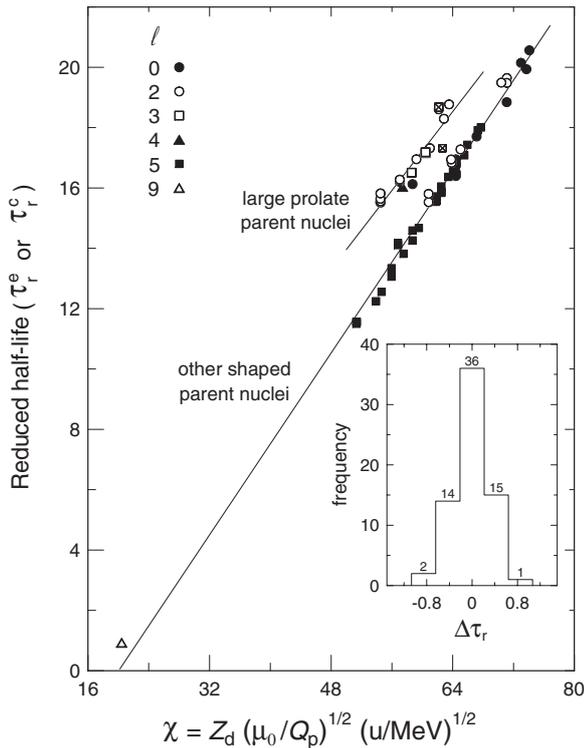
Fig. 4. Reduced half-life, τ_r, plotted against the quantity $\chi = Z_d(\mu_0/Q_p)^{1/2}$; τ_r is defined as the difference $\tau - (\tau_0 + \tau_1 + \tau_2^{ce})$ between the half-life, τ, and the sum of the three partial contributions to τ defined by eqs. (21), (22), and (29). Symbols represent experimental reduced half-lives, τ_r^e, for different values of ℓ as indicated. The calculated reduced half-life, τ_r^c, is given by the least-squares straight lines through the points for large prolate deformed parent nuclei (upper line), and other shaped nuclei (lower line) as indicated (see eq. (31)). The inset shows the distribution of the deviation $\Delta\tau_r = \tau_r^c - \tau_r^e$ where 92% of the experimental data are reproduced within a factor 3. The symbol $\boxtimes$ indicates data which deviate from the upper line by a factor greater than 4.5. The case for ^{53m}Co (open triangle) is underestimated by a factor 6.

linear trends are shown indeed independent upon ℓ-values. Linear least-squares fitting procedures have been applied to both sets of data points, thus obtaining

$$\tau_r^c = \alpha(\chi - \beta), \qquad \chi = Z_d(\mu_0/Q_p)^{1/2}, \qquad (31)$$

where $\alpha = 0.327$, $\beta = 7.27$, $g = 0$, and $\sigma = 0.30$ for the upper line (large prolate cases), with one measurement differing by a factor 5 (^{117}La, $\ell = 2$), and another one by a factor 6 (^{140}Ho, $\ell = 3$); $\alpha = 0.377$, $\beta = 20.0$, $g = 0.12$, and $\sigma = 0.29$ for the lower line, with one measurement differing by a factor 4.7 (^{170}Au, $\ell = 2$), and the case for ^{53m}Co ($\ell = 9$), for which case the calculated half-life resulted underestimated by a factor 6 (fig. 4). The present results can be considered very satisfactory in view of only four measurements (of only two cases) in seventy-one showing deviation between calculated and measured half-life values greater than a factor about 5.

4 Discussion

The present analysis shows interesting features. Firstly, two quite different values for the parameter g have been found, namely, $g = 0$ for the set of large prolate-shaped parent nuclei ($\delta \gtrsim 0.1$), and $g = 0.12$ for other shaped ($\delta \lesssim 0.1$) proton emitters. The former g-value probably indicates that the equivalent spherical nucleus (volume conservation) to a very prolate, neutron-deficient nucleus of $Q_p > 0$ does not need an overlapping region, *i.e.* the excess proton to be emitted from the deformed nucleus should be found very probably at the nuclear surface, near to one of the opposite poles of the ellipsoidal-shaped parent nucleus, where the Coulomb barrier is minimum. Other shaped nuclei, on the contrary, seems to correspond to equivalent spherical-shaped nuclei with a very narrow (but not null) overlapping region to describe the "arrival" of the proton at the nuclear surface, *i.e.* the proton was not yet "ready" to escape the nucleus. These differences between each group of nuclei ($\delta \gtrsim 0.1$ and $\delta \lesssim 0.1$) may explain, in a qualitative way, the two linear, clearly separated trends depicted in fig. 4. Anyway, it should be remarked that the calculated half-life values, $T_{1/2_p}^c$, are not so strongly sensitive to small values of the parameter g (straightforward calculation indicates indeed that a variation from $g \approx 0$ to $g \approx 0.20$ can cause a maximum increase by a factor 2 in the half-life). This is a consequence of the small contribution to half-life (τ_1, eq. (22)) due to a very narrow overlapping barrier region in proton decay.

An intriguing case is that for ^{53m}Co, for which case one has $\ell = 9$, $x \approx 37$, $y \approx 2$, and $x/y^2 \approx 9.3$, *i.e.* $x/y^2 \gg 1$, therefore the series expansion (24) with only two terms is not sufficient to separate completely the centrifugal contribution to half-life from the Coulomb contribution. Even so ^{53m}Co (open triangle in fig. 4) fits reasonably well to the lower line, in agreement with its predicted nearly spherical shape ($\delta = 0.077$ [49]) and the high-spin $19/2^-$ assigned to this isomeric state [1,62]. We think, however, this case merits a detailed investigation in a future.

Tables 2 and 3 list all information concerning proton radioactivity for isomeric and ground-state transitions, respectively. Columns two to five contain the input data to the present analysis. Column eight shows the difference $\Delta\tau = \tau^c - \tau^e = \Delta\tau_r = \tau_r^c - \tau_r^e$ between calculated and experimental half-life values as obtained in this work, where τ_r^c are given by the least-squares straight lines (31). Finally, for the sake of comparison, columns nine and ten list the results obtained from the systematics by Delion *et al.* [4]. We remark that both systematic analyses were able to detect the same cases of greater deviations, namely, ^{141m}Ho ($\delta \approx 0.24$) in table 2, and ^{117}La ($\delta = 0.24$) and ^{140}Ho ($\delta = 0.25$) in table 3, *i.e.* cases of large deformation of the parent nucleus. Altogether, the $\Delta\tau$-values from the present analysis (column eight in tables 2 and 3) correspond to a standard deviation $\sigma = 0.34$, which compares with $\sigma = 0.38$ from data of ref. [4] as listed in columns nine and ten. If, however, the three cases of greater deviations just mentioned plus the result for ^{53m}Co in table 2 are removed then σ drops equally to 0.27 for both systematics

Table 2. Properties of known isomeric proton transitions.

		Degree of deformation $\delta^{(a)}$	Q_p-value[b] (MeV)	$\ell^{(c)}$	Half-life values				
					Experimental[c] $T^e_{1/2_p}$(s)	Calculated, $T^c_{1/2_p}$(s)			
No.	Isomer					This work	$\Delta\tau^{(d)}$	Ref. [4]	$\Delta\tau^{(d)}$
1	$^{53m}_{27}$Co	0.077	1.599	9	1.65×10^1	4.02×10^0	−0.78	—	—
2	$^{117m}_{57}$La	0.242	0.951	4	1.0×10^{-2}	2.2×10^{-2}	0.34	—	—
3	$^{141m}_{67}$Ho	0.239	1.264	0	0.66×10^{-5}	3.1×10^{-5}	0.67	4.7×10^{-5}	0.85
4	$^{146m}_{69}$Tm	−0.140	1.150	5	3.5×10^{-1}	3.2×10^{-1}	−0.04	3.1×10^{-1}	−0.06
5	$^{147m}_{69}$Tm	−0.134	1.134	2	3.6×10^{-4}	1.7×10^{-4}	−0.33	1.7×10^{-4}	−0.33
6	$^{150m}_{71}$Lu	−0.117	1.325	2	3.0×10^{-5}	1.1×10^{-5}	−0.44	1.4×10^{-5}	−0.33
7	$^{151m}_{71}$Lu	−0.111	1.325	2	1.6×10^{-5}	1.1×10^{-5}	−0.16	1.0×10^{-5}	−0.20
8	$^{156m}_{73}$Ta	−0.039	1.146	5	0.89×10^1	0.68×10^1	−0.12	1.1×10^1	0.09
9	$^{161m}_{75}$Re	0.062	1.336	5	3.25×10^{-1}	3.03×10^{-1}	−0.03	2.8×10^{-1}	−0.06
10	$^{164m}_{77}$Ir	0.069	1.847	5	1.1×10^{-4}	1.7×10^{-4}	0.19	—	—
11					0.58×10^{-4}		0.47		—
12	$^{165m}_{77}$Ir	0.078	1.747	5	3.5×10^{-4}	7.0×10^{-4}	0.30	—	—
13	$^{166m}_{77}$Ir	0.084	1.347	5	0.84×10^0	0.94×10^0	0.05	1.1×10^0	0.12
14	$^{167m}_{77}$Ir	0.091	1.262	5	7.5×10^0	6.5×10^0	−0.06	7.1×10^0	−0.02
15	$^{170m}_{79}$Au	−0.070	1.767	5	0.84×10^{-3}	1.7×10^{-3}	0.31	—	—
16					1.8×10^{-3}		−0.02		—
17	$^{171m}_{79}$Au	−0.076	1.718	5	2.2×10^{-3}	3.5×10^{-3}	0.20	3.2×10^{-3}	0.16
18	$^{177m}_{81}$Tl	−0.039	1.987	5	4.5×10^{-4}	2.4×10^{-4}	−0.27	2.1×10^{-4}	−0.33
19					5.3×10^{-4}		−0.34		−0.40
20	$^{185m}_{83}$Bi	−0.039	1.624	0	4.4×10^{-5}	3.4×10^{-5}	−0.11	—	—
21					5.9×10^{-5}		−0.24		—

[a] Degree of nuclear deformation as given by $\delta = 0.757\beta_2 + 0.273\beta_2^2$, where β_2 is the parameter of quadrupole deformation, the values of which are taken from [49].

[b] Q_p-values emerge from eq. (13) with mass-excess values taken from [41].

[c] Angular momentum, ℓ, and experimental half-life values, $T^e_{1/2_p}$(s), are from [4,7,11,41] and references quoted therein.

[d] $\Delta\tau = \tau^c - \tau^e = \log_{10}(T^c_{1/2_p}/T^e_{1/2_p})$.

(this means that $\sim 92\%$ of the measurements are reproduced within a factor ~ 3). Therefore, we can conclude that our semiempirical analysis developed in the precedent sections compares quite completely with that by Delion *et al.* [4].

The goodness in reproducing the experimental proton decay half-life data attained in the present analysis has encouraged us to make predictions for a few cases of proton emission not yet accessed experimentally. Although being this a delicate matter we venture into making predictions for a few cases. Results are listed in table 4. The case for ^{105}Sb has been included to show why it should not be considered nowadays a proton emitter. Half-life predictions as reported in table 4 are to be seen of course with reserve, and they must be considered as only indicative values since they can be affected to some extent by uncertainties coming mainly from difficulties at defining precise values for both Q_p and ℓ, as well as the amount of deformation exhibited by the parent nucleus in each case. Certainly it would be remarkable whether some $Z < 50$

ground-state proton emitters like ^{30}Cl, ^{58}Ge, ^{68}Br, or even ^{89}Rh could be detected.

5 Final remarks and conclusion

A semiempirical, one-parameter model developed recently by us [6,33,35] has been applied here to analyse in a systematic way all available half-life values measured for both the ground-state and isomeric proton transitions. From this analysis half-life predictions for a few cases of proton decay not yet measured have been made and found in the range $\sim 7\,\mu$s–40 s (table 4). The analogy to alpha decay is quite complete, differing only in the quantitative aspects of the physical quantities involved in the description of the decay process such as a) a relatively low Q-value for proton decay ($Q_p \lesssim 2\,$MeV), b) very unstable proton bound systems, c) an average proton radius of $0.87 \pm 0.02\,$fm adopted throughout the calculations, d) a contribution to Q_p-value not greater than 20 keV coming from the nuclear

Table 3. Properties of known ground-state proton transitions.

No.	Parent nucleus	Degree of deformation $\delta^{(a)}$	Q_p-value[(b)] (MeV)	$\ell^{(c)}$	Experimental[(c)] $T^e_{1/2_p}$(s)	Calculated, $T^c_{1/2_p}$(s) This work	$\Delta\tau^{(d)}$	Ref. [4]	$\Delta\tau^{(d)}$
1	$^{109}_{53}$I	0.128	0.830	2	$1.07 \times 10^{-4(e)}$	1.05×10^{-4}	-0.01	0.83×10^{-4}	-0.11
2	$^{112}_{55}$Cs	0.169	0.830	2	5.0×10^{-4}	5.2×10^{-4}	0.02	7.6×10^{-4}	0.18
3	$^{113}_{55}$Cs	0.168	0.980	2	$1.67 \times 10^{-5(e)}$	1.35×10^{-5}	-0.09	0.66×10^{-5}	-0.40
4	$^{117}_{57}$La	0.242	0.811	2	$2.2 \times 10^{-2(e)}$	4.6×10^{-3}	-0.68	0.61×10^{-2}	-0.61
5	$^{121}_{59}$Pr	0.268	0.851	2	1.0×10^{-2}	0.73×10^{-2}	-0.14	3.3×10^{-3}	-0.48
6	$^{130}_{63}$Eu	0.280	1.033	2	0.90×10^{-3}	1.53×10^{-3}	0.23	3.1×10^{-3}	0.54
7	$^{131}_{63}$Eu	0.280	0.953	2	2.66×10^{-2}	1.06×10^{-2}	-0.40	3.13×10^{-2}	0.07
8	$^{135}_{65}$Tb	0.275	1.193	3	0.94×10^{-3}	1.70×10^{-3}	0.26	2.2×10^{-3}	0.36
9	$^{140}_{67}$Ho	0.249	1.110	3	0.60×10^{-2}	3.7×10^{-2}	0.79	0.95×10^{-1}	1.20
10	$^{141}_{67}$Ho	0.239	1.194	3	$4.20 \times 10^{-3(e)}$	6.3×10^{-3}	0.18	1.1×10^{-2}	0.42
11	$^{145}_{69}$Tm	0.205	1.754	5	$3.5 \times 10^{-6(e)}$	5.8×10^{-6}	0.22	4.1×10^{-6}	0.07
12	$^{146}_{69}$Tm	-0.140	1.208	5	$7.50 \times 10^{-2(e)}$	8.0×10^{-2}	0.03	6.7×10^{-2}	-0.05
13	$^{147}_{69}$Tm	-0.134	1.064	5	4.30×10^{0}	3.04×10^{0}	-0.15	2.39×10^{0}	-0.25
14	$^{150}_{71}$Lu	-0.117	1.285	5	$4.9 \times 10^{-2(e)}$	5.9×10^{-2}	0.08	5.4×10^{-2}	0.04
15	$^{151}_{71}$Lu	-0.111	1.255	5	$1.30 \times 10^{-1(e)}$	1.14×10^{-1}	-0.06	1.02×10^{-1}	-0.10
16	$^{155}_{73}$Ta	-0.006	1.786	5	1.2×10^{-5}	3.9×10^{-5}	0.51	2.7×10^{-5}	0.35
17	$^{156}_{73}$Ta	-0.039	1.026	2	$1.65 \times 10^{-1(e)}$	0.94×10^{-1}	-0.24	1.2×10^{-1}	-0.14
18	$^{157}_{73}$Ta	0.035	0.946	0	3.0×10^{-1}	1.8×10^{-1}	-0.22	2.77×10^{-1}	-0.03
19	$^{159}_{75}$Re	0.041	1.836	5	2.1×10^{-5}	6.2×10^{-5}	0.47	—	—
20	$^{160}_{75}$Re	0.062	1.296	2	0.87×10^{-3}	4.05×10^{-4}	-0.33	0.65×10^{-3}	-0.13
21	$^{161}_{75}$Re	0.062	1.216	0	3.7×10^{-4}	4.0×10^{-4}	0.03	5.7×10^{-4}	0.19
22	$^{166}_{77}$Ir	0.084	1.167	2	1.5×10^{-1}	4.5×10^{-2}	-0.52	—	—
23	$^{167}_{77}$Ir	0.091	1.086	0	1.1×10^{-1}	0.68×10^{-1}	-0.21	1.1×10^{-1}	0
24	$^{170}_{79}$Au	-0.070	1.497	2	$3.6 \times 10^{-4(e)}$	1.2×10^{-4}	-0.48	—	—
25	$^{171}_{79}$Au	-0.076	1.468	0	$3.7 \times 10^{-5(e)}$	3.5×10^{-5}	-0.02	4.5×10^{-5}	0.08
26	$^{176}_{81}$Tl	-0.039	1.268	0	5.2×10^{-3}	1.3×10^{-2}	0.40	—	—
27	$^{177}_{81}$Tl	-0.039	1.180	0	0.67×10^{-1}	1.26×10^{-1}	0.27	2.1×10^{-1}	0.50

[(a)] Degree of nuclear deformation as given by $\delta = 0.757\beta_2 + 0.273\beta_2^2$, where β_2 is the parameter of quadrupole deformation, the values of which are taken from [49].

[(b)] Q_p-values emerge from eq. (13) with mass-excess values taken from [41].

[(c)] Angular momentum, ℓ, and experimental half-life values, $T^e_{1/2_p}$(s), are from [4,5,7,11,41] and references quoted therein.

[(d)] $\Delta\tau = \tau^c - \tau^e = \log_{10}(T^c_{1/2_p}/T^e_{1/2_p})$.

[(e)] Selected value, among various reported measurements, to give the least deviation $\Delta\tau$.

screening by the surrounding electrons in both the parent and daughter nuclei, e) a very narrow overlapping barrier region leading, therefore, to a probability of finding of the proton at the nuclear surface close to unity, and f) a strong dependence of tunneling through the external potential barrier upon mutual angular momentum.

A number of proton emission cases experimentally investigated, summing up to nearly seventy measured half-life values, have been analysed in a systematic way. The effect of nuclear deformation was clearly manifested after plotting the purely Coulomb contribution to half-life against the Coulomb parameter $Z_d(\mu_0/Q_p)^{1/2}$ following a similar procedure introduced by Delion *et al.* [4]. In this way, the data resulted grouped into two categories of nuclei, namely, largely prolate-shaped parent nucleus of degree of deformation $\delta \gtrsim 0.1$, and other shaped ones ($\delta \lesssim 0.1$), in both cases showing no dependence upon ℓ-values. For the former group of proton emitters the best

Table 4. Half-life predictions of ground-state proton radioactivity for cases not yet experimentally observed.

No.	Parent nucleus				Mass excesses, ΔM (MeV)[b]		Q_p-value[c]	ℓ[d]	Proton-decay	Other modes of
	Element	Z	A	δ[a]	Parent	Daughter	(MeV)		half-life[e]	decay and half-life[b]
1	Cl	17	30	-0.156	4.44	-3.16	0.313	6	2 ms	?
2	Ge	32	58	0.178	-8.37	-15.90	0.245	1	2.4 ms	?
3	Br	35	68	-0.211	-38.64	-46.49	0.566	5	12 μs	?
4	Rh	45	89	0.041	-47.66	-55.65	0.708	4	7 μs	?
5	Sb	51	105	0.063	-63.82	-71.59	0.489[f]	2	250 ms	?, 1.12 s
6							0.356		3.5 h	
7	I	53	108	0.121	-52.65	-60.54	0.610	2	160 ms	?, 36 ms
8								4	41 s	
9	Au	79	173	-0.076	-12.82	-21.101	1.008	0	4.4 s	α, β^+, 25 ms
10	Bi	83	184	-0.039	1.05	-7.569	1.348	1	16 ms	α(?), 6.6 ms
11	Bi	83	186	-0.039	-3.17	-11.541	1.100	1	12 s	α, 14.8 ms

[a] This is the amount of nuclear quadrupole deformation as defined in tables 2 and 3.
[b] Values taken from ref. [41].
[c] Screening effect included (see eq. (13)).
[d] Deduced from spin and parity values reported in ref. [41].
[e] Uncertainties (only statistical) amount to a factor 4.
[f] This case has been experimentally reinvestigated quite recently [63,64], thus showing that ^{105}Sb should be excluded from being a proton-emitter nuclide. The reported, new Q_p-value is 0.356 ± 0.022 MeV [64].

value for the adjustable parameter of the model was $g = 0$, *i.e.* no overlapping barrier to the equivalent spherical parent nucleus was necessary to fit the reduced data. For the other group it gave $g = 0.12$, showing that there is a contribution, although very small, from a narrow potential barrier in the overlapping region. In spite of a still relatively small number of measurements available, the present analysis developed in the framework of Gamow's tunnelling mechanism leads to a standard deviation $\sigma = 0.34$ for the quantity $\tau = \log_{10} T_{1/2_\mathrm{p}}$ with only four measurements that deviate from the systematics by a factor 4–6 (we remind that in alpha decay systematics values of σ have been obtained in the range ~ 0.20–0.32 [6,33,35]).

Since an early past, strong correlations between half-life (or decay constant) and the energy of the emitted particle (known as Geiger-Nuttall's plots [65]) have been established, originally observed for alpha decay processes in natural radioactivity of heavy elements. The same happens to proton radioactivity, therefore complementing the analogy to alpha decay. Examples are depicted in fig. 5, where straight lines fit completely (in a log-scale) the half-life values plotted against the quantity $Q_\mathrm{p}^{-1/2}$ for a given isotopic sequence of proton-emitter nuclides and the same ℓ-value. In spite of a limited number of measurements we succeeded in constructing the trend τ *vs.* $Q_\mathrm{p}^{-1/2}$ for a few cases. As Z increases the lines dislocate towards up-left in the same way as it happens in alpha decay [6,33]. The sequences for Ir and Tm (all cases of $\ell = 5$ transitions) display 5 and 6 orders of magnitude in the half-life, respectively, appearing as quite perfect examples of true Geiger-Nuttall's law.
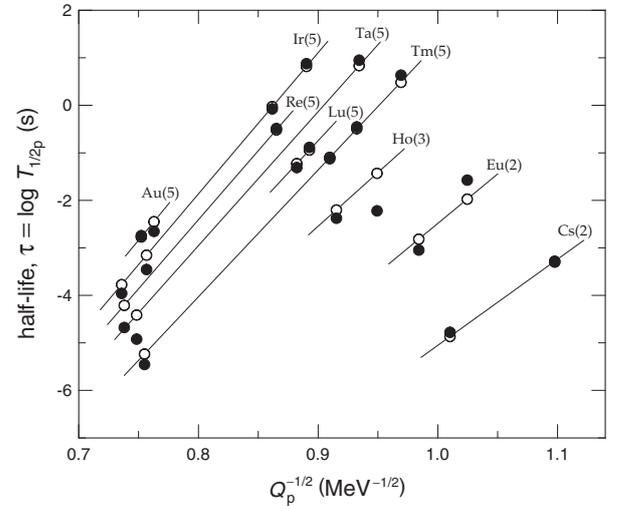

Fig. 5. Geiger-Nuttall plots for different cases of proton radioactivity. The quantity $\tau = \log_{10} T_{1/2_\mathrm{p}}$(s) is plotted against $Q_\mathrm{p}^{-1/2}$ for a number of isotopic sequences and ℓ-values indicated (in parenthesis) near the lines. Experimental data are represented by full symbols, and open ones indicate calculated results by the present approach.

As conclusion, the present analysis of half-life for proton radioactivity enabled us to calculate and systematize all decay data, including both the ground-state and isomeric proton transitions, with a quite satisfactory level of fitting, reaching a standard deviation $\sigma = 0.34$, thus

comparable to alpha decay cases. The present systematics provides, in our opinion, a rather satisfactory global description of proton radioactivity giving, in addition, predictions for new, possible cases of measurable half-lives which can be accessed taking advantage of the present and/or novel experimental techniques.

References

1. K.P. Jackson, C.U. Cardinal, H.C. Evans, N.A. Jelley, J. Cerny, Phys. Lett. B **33**, 281 (1970).
2. J. Cerny, J.E. Esterl, R.A. Gough, R.G. Sextro, Phys. Lett. B **33**, 284 (1970).
3. A.A. Sonzogni, Nucl. Data Sheets **95**, 1 (2002).
4. D.S. Delion, R.J. Liotta, R. Wyss, Phys. Rev. Lett. **96**, 072501 (2006).
5. D.T. Joss *et al.*, Phys. Lett. B **641**, 34 (2006).
6. O.A.P. Tavares, E.L. Medeiros, M.L. Terranova, J. Phys. G: Nucl. Part. Phys. **31**, 129 (2005).
7. P.J. Woods, C.N. Davids, Annu. Rev. Nucl. Part. Sci. **47**, 541 (1997).
8. S. Åberg, P.B. Semmes, W. Nazarewicz, Phys. Rev. C **56**, 1762 (1997); **58**, 3011 (1998).
9. E. Maglione, L.S. Ferreira, Eur. Phys. J. A **15**, 89 (2002).
10. L.S. Ferreira, E. Maglione, J. Phys. G: Nucl. Part. Phys. **31**, S1569 (2005).
11. D.S. Delion, R.J. Liotta, R. Wyss, Phys. Rep. **424**, 113 (2006).
12. K.P. Rykaczewski, Eur. Phys. J. A **15**, 81 (2002).
13. M. Karny *et al.*, Phys. Rev. Lett. **90**, 012502 (2003).
14. T.N. Ginter *et al.*, Phys. Rev. C **68**, 034330 (2003).
15. H. Kettunen *et al.*, Phys. Rev. C **69**, 054323 (2004).
16. P.J. Sellin, P.J. Woods, T. Davinson, N.J. Davis, K. Livingston, R.D. Page, A.C. Shotter, Phys. Rev. C **47**, 1933 (1993).
17. S. Hofmann, W. Reisdorf, G. Münzenberg, F.P. Heßberger, J.R.H. Schneider, Z. Phys. A **305**, 111 (1982).
18. O. Klepper, T. Batsch, S. Hofmann, R. Kirchner, W. Kurcewicz, W. Reisdorf, E. Roeckl, D. Schardt, G. Nyman, Z. Phys. A **305**, 125 (1982).
19. A.P. Robinson, P.J. Woods, D. Seweryniak, C.N. Davids, M.P. Carpenter, A.A. Hecht, D. Peterson, S. Sinha, W.B. Walters, S. Zhu, Phys. Rev. Lett. **95**, 032502 (2005).
20. C.R. Bingham *et al.*, Nucl. Instrum. Methods Phys. Res. B **241**, 185 (2005).
21. J.C. Batchelder *et al.*, Eur. Phys. J. A **25**, s01, 149 (2005).
22. D.N. Basu, P. Roy Chowdhury, C. Samanta, Phys. Rev. C **72**, 051601 (R) (2005).
23. M. Balasubramaniam, N. Arunachalam, Phys. Rev. C **71**, 014603 (2005).
24. A.T. Kruppa, B. Barmore, W. Nazarewicz, T. Vertse, Phys. Rev. Lett. **84**, 4549 (2000).
25. B. Barmore, A.T. Kruppa, W. Nazarewicz, T. Vertse, Phys. Rev. C **62**, 054315 (2000).
26. H. Esbensen, C.N. Davids, Phys. Rev. C **63**, 014315 (2000).
27. B. Barmore, A.T. Kruppa, W. Nazarewicz, T. Vertse, Nucl. Phys. A **682**, 256c (2001).
28. C.N. Davids, H. Esbensen, Prog. Theor. Phys. Suppl. **146**, 358 (2002).
29. C.N. Davids, H. Esbensen, Phys. Rev. C **69**, 034314 (2004).
30. D. Seweryniak *et al.*, Eur. Phys. J. A **25**, s01, 159 (2005).
31. D. Seweryniak *et al.*, J. Phys. G: Nucl. Part. Phys. **31**, S1503 (2005).
32. P. de Marcillac, N. Coron, G. Dambier, J. Leblanc, J.P. Moalic, Nature **422**, 876 (2003).
33. O.A.P. Tavares, M.L. Terranova, E.L. Medeiros, Nucl. Instrum. Methods Phys. Res. B **243**, 256 (2006).
34. O.A.P. Tavares, M.L. Terranova, Radiat. Meas. **27**, 19 (1997).
35. E.L. Medeiros, M.M.N. Rodrigues, S.B. Duarte, O.A.P. Tavares, J. Phys. G: Nucl. Part. Phys. **32**, B23 (2006).
36. E.L. Medeiros, M.M.N. Rodrigues, S.B. Duarte, O.A.P. Tavares, J. Phys. G: Nucl. Part. Phys. **32**, 2345 (2006).
37. F.A. Danevich *et al.*, Phys. Rev. C **67**, 014310 (2003).
38. Yu.G. Zdesenko, F.T. Avignone III, V.B. Brudanin, F.A. Danevich, S.S. Nagorny, I.M. Solsky, V.I. Tretyak, Nucl. Instrum. Methods Phys. Res. A **538**, 657 (2005).
39. P. Belli *et al.*, Nucl. Phys. A **789**, 15 (2007).
40. O.A.P. Tavares, E.L. Medeiros, Phys. Scr. **76**, C163 (2007).
41. G. Audi, O. Bersillon, J. Blachot, A.H. Wapstra, Nucl. Phys. A **729**, 3 (2003).
42. K-N. Huang, M. Aoyagi, M.H. Chen, B. Crasemann, H. Mark, At. Data Nucl. Data Tables **18**, 243 (1976).
43. P. Mergell, Ulf-G. Meißner, D. Drechsel, Nucl. Phys. A **596**, 367 (1996).
44. G.G. Simon, Ch. Schmitt, F. Borkowski, V.H. Walther, Nucl. Phys. A **333**, 381 (1980).
45. F. Borkowski, G.G. Simon, V.H. Walther, R.D. Wendling, Nucl. Phys. B **93**, 461 (1975).
46. I. Sick, Phys. Lett. B **576**, 62 (2003).
47. K. Melnikov, T. van Ritbergen, Phys. Rev. Lett. **84**, 1673 (2000).
48. W.D. Myers, *Droplet Model of Atomic Nuclei* (Plenum, New York, 1977).
49. P. Möller, J.R. Nix, W.D. Myers, W.J. Swiatecki, At. Data Nucl. Data Tables **59**, 185 (1995).
50. R.D. Page, P.J. Woods, R.A. Cunningham, T. Davinson, N.J. Davis, S. Hofmann, A.N. James, K. Livingston, P.J. Sellin, A.C. Shotter, Phys. Rev. Lett. **68**, 1287 (1992).
51. R.D. Page *et al.*, Phys. Rev. Lett. **72**, 1798 (1994).
52. R.D. Page *et al.*, Phys. Rev. C **53**, 660 (1996).
53. H. Mahmud, C.N. Davids, P.J. Woods, T. Davinson, A. Heinz, J.J. Ressler, K. Schmidt, D. Seweryniak, J. Shergur, A.A. Sonzogni, W.B. Walters, Eur. Phys. J. A **15**, 85 (2002).
54. C.N. Davids *et al.*, Phys. Rev. C **55**, 2255 (1997).
55. C.N. Davids *et al.*, Phys. Rev. Lett. **80**, 1849 (1998).
56. C.N. Davids, P.J. Woods, H. Mahmud, T. Davinson, A. Heinz, J.J. Ressler, K. Schmidt, D. Seweryniak, J. Shergur, A.A. Sonzogni, W.B. Walters, Phys. Rev. C **69**, 011302 (2004).
57. P.J. Woods, P. Munro, D. Seweryniak, C.N. Davids, T. Davinson, A. Heinz, H. Mahmud, F. Sarazin, J. Shergur, W.B. Walters, A. Woehr, Phys. Rev. C **69**, 051302(R) (2004).
58. K. Rykaczewski *et al.*, Phys. Rev. C **60**, 011301 (1999).
59. J.R. Irvine, C.N. Davids, P.J. Woods, D.J. Blumenthal, L.T. Brown, L.F. Conticchio, T. Davinson, D.J. Henderson, J.A. Mackenzie, H.T. Penttilä, D. Seweryniak, W.B. Walters, Phys. Rev. C **55**, R1621 (1997).
60. G.L. Poli *et al.*, Phys. Rev. C **59**, R2979 (1999).

61. G.L. Poli *et al.*, Phys. Rev. C **63**, 044304 (2001).
62. J. Cerny, R.A. Gough, R.G. Sextro, J.E. Esterl, Nucl. Phys. A **188**, 666 (1972).
63. Z. Liu *et al.*, Phys. Rev. C **72**, 047301 (2005).
64. C. Mazzocchi *et al.*, Phys. Rev. Lett. **98**, 212501 (2007).
65. H. Geiger, J.M. Nuttall, Philos. Mag. **22**, 613 (1911); H. Geiger, Z. Phys. **8**, 45 (1921).